P3.1 CONTRIBUTIONS FROM CALIFORNIA COASTAL-ZONE SURFACE FLUXES TO HEAVY COASTAL PRECIPITATION: A CASE STUDY FROM AN EL NIÑO YEAR

P. Ola G. Persson[1], B. Walter[3], P. J. Neiman[2], and F. M. Ralph[2]

[1]Cooperative Institute for Research in Environmental Sciences/NOAA/ETL, Boulder, CO
[2]NOAA/Environmental Technology Laboratory, Boulder, CO
[3]NorthWest Research Associates, Bellevue, WA

1. INTRODUCTION

Surface fluxes of sensible heat, moisture and momentum over the oceans have long been thought to play a significant role in the modulation of the evolution of maritime extratropical cyclones and of the precipitation processes within these storms. In particular, the surface moisture flux provides a direct source of the moisture needed for precipitation, while the sensible heat flux can affect the stability of the storm environment, thereby modulating the precipitation process and amount.

Various studies, most relying on numerical models, have shown that the degree to which surface sensible heat and moisture fluxes affect storm evolution and precipitation depends on the location and timing of these fluxes relative to the cyclone and its associated structures (Reed and Albright, 1986; Kuo and Reed, 1988; Kuo *et al,* 1991; Langland *et al,* 1995). In addition, the magnitude and even the sign of the impact depend on the relative temperatures of the ocean and the atmosphere. Hence, storms of comparable magnitude and thermodynamic characteristics will be impacted differently over different oceanic regions. Storms passing over the relatively high sea-surface temperatures (SSTs) of the Gulf Stream in the western Atlantic Ocean will be enhanced to a much greater extent than a similar storm occurring over the relatively cooler waters off the west coast of the United States.

The SST can vary temporally as well as spatially, and this usually occurs on much larger time scales than that of the individual storms. A well-known example of temporal SST changes is that occurring with the El Niño-Southern Oscillation (ENSO). During the warm phase of a strong ENSO, such as occurred in 1983 and again in 1998, the SSTs in the central Pacific Ocean are anomalously cold, while the SSTs within 300 km of the California coast are anomalously warm. Hence, if the coastal surface sensible heat and moisture fluxes are important for storm development and precipitation, one might expect a different impact during a strong warm ENSO phase compared to other phases of the ENSO.

The California Landfalling Jets Experiment (CALJET; Ralph *et al*., 1999) conducted its field program over the coastal and offshore waters of California during the strong, warm ENSO phase of 1998. This paper will present the case of February 3, 1998, for which the observed surface sensible and latent heat fluxes within 150 km of the shore within a moderate low-level jet are shown to significantly contribute to the destabilization of the air just before it is forced to ascend the steep coastal terrain. As the air ascends, deep convection occurs with significant coastal flooding as result. A bulk surface flux parameterization is shown to match direct surface flux measurements reasonably well in this case, and is used to extend the results to suggest that the coastal fluxes only enhance the coastal precipitation during years with anomalously warm SSTs (ENSO years) and may even help suppress coastal convection during years of more normal colder SSTs.

2. DATA SET AND SYNOPTIC DESCRIPTION

The large integrated CALJET observational network featured the NOAA P-3 aircraft and a coastal array of 915 MHz wind profilers, and is described by Ralph *et al*. (1999). On Feb. 3, the aircraft flew between 1140-1930 UTC. It made measurements in the Santa Barbara Channel near 1230-1300 UTC, followed by a dropsonde cross-section and flux stacks about 140 km further south between 1330-1600 UTC. It then returned to the Santa Barbara Channel region between 1630-1800 UTC.

For the storm of February 2-3, 1998, phasing of a surface baroclinic zone with an upper-level circulation center led to cyclogenesis roughly 1000 km offshore (Persson *et al.*, 1999a; Ralph *et al.*, 1999). The storm had a complex mesoscale structure and a low-level jet (LLJ) region containing winds over 40 m/s near 1 km in altitude. It deepened as it approached the California

Corresponding author: Dr. Ola Persson, CIRES/NOAA/ETL,R/ET7 325 Broadway, Boulder, CO 80305. E-mail: opersson@etl.noaa.gov

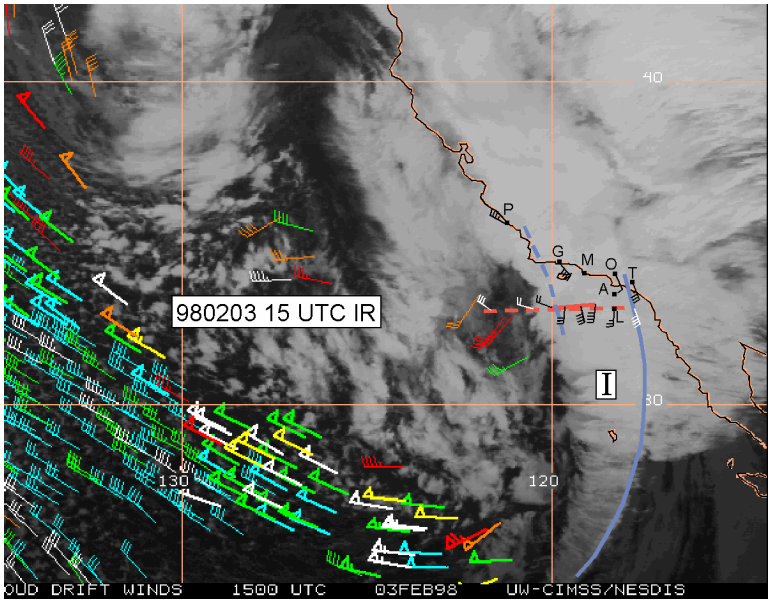

Fig. 1: IR image and mid-level cloud-track winds at 1500 UTC Feb. 3, 1998. The primary (solid) and secondary (dashed) cold fronts are shown in blue. The dashed red line shows the approximate track of the P-3 aircraft between 1300-1605 UTC, while the wind flags on this track show low-level winds measured in-situ or by dropsondes. The coastal wind profiler sites of Pt. Piedras Blancas (P), Goleta (G), Santa Catalina (A), Oxnard (O), and Tustin (T) are shown, with low-level winds shown at four of these sites. The Pt. Mugu (M) rawinsonde site is also shown.

coastline. In some areas of the Southern California coastal mountains, 24-h precipitation totals from this storm exceeded 300 mm (12 inches) resulting in flooding and mudslides. The storm also forced the closure of Los Angeles International Airport.

Complex interactions occurred between the coastal orography in the California Bight region and the landfalling storm on Feb. 3 (Neiman *et al.*, 2002). A prefrontal squall line and a primary cold front brought the initial heavy precipitation. A secondary cold front produced brief but very intense precipitation in the coastal mountains along the northern shore of the California Bight (Fig.1).

Detailed in-situ thermodynamic and flux measurements were obtained in the 15-20 m/s LLJ ahead of this secondary front about 140 km offshore between 1430-1605 UTC and later near the shore between 1730-1830 UTC, as described by Persson *et al.* (1999b) (see also Fig 6). The offshore measurements showed a bubble of warm, moist air ahead of the secondary cold front (Fig. 2a), with a weak warm-frontal feature to the east of this bubble. In the 2.5 hours between the offshore and nearshore measurements, this bubble of warm, moist air advected towards the coast to the NNE, keeping just to the east of the secondary cold front as it advected eastward. This is illustrated schematically in Fig. 3. Hence, the nearshore sampling by the P-3 occurred in

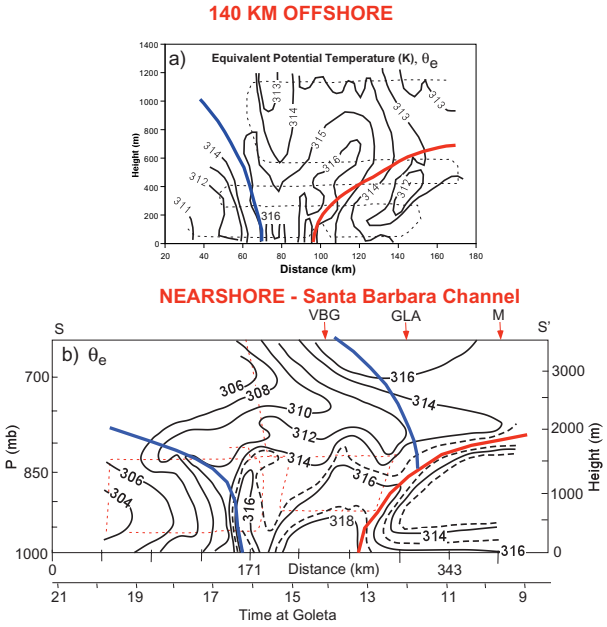

Fig. 2: a) Offshore and b) nearshore θ_e cross-sections. In a), a velocity of 16.8 ms^{-1} from 200° was used in the time-to-space conversion of the aircraft data. In b), the analysis was done using the aircraft data collected near 1230 UTC and near 1730 UTC, data from buoys in the Santa Barbara Channel and 3 rawinsondes from Goleta and Pt. Mugu (arrows). A velocity of 9.2 m/s from 270° was used in the time-to-space conversion. The location of b) is marked by S-S' in Fig. 3. The aircraft tracks are shown as faint dashed lines.

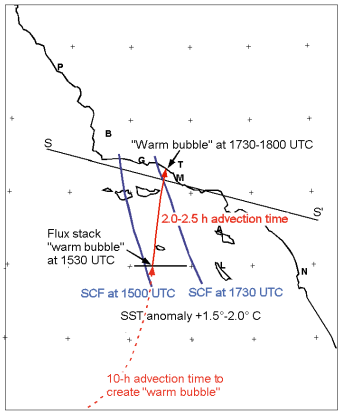

Fig 3: Schematic of the parcel trajectory from the offshore cross-section to the north coast of the California Bight. The heavy blue lines represent the secondary cold front at the two times indicated.

approximately the same air that was sampled offshore. Figure 2b shows the nearshore θ_e analysis valid near 1800 UTC along the line S-S' indicated in Fig. 3. This analysis represents the nearshore environment after the merger of the secondary cold front with the low-level remnant of the primary cold-front that had apparently been retarded by the blocking effects of the coastal orography. Neiman *et al*. (2002) explain the complex evolution in more detail. This analysis shows the warm, moist bubble of air still ahead of the secondary cold front.

3. FLUXES AND FLUX IMPACT

Between 1430-1605 UTC, the P-3 aircraft performed a flux stack just ahead of the secondary cold front about 140 km south of the coastline near Goleta. This flux stack consisted of 5 level aircraft passes (or legs) approximately perpendicular to the frontal orientation and the low-level winds. The legs were done in descending order between 1154 m and 66 m. In addition to the standard 1-s flight level measurements, data was also collected at 40 Hz in order to observe turbulent structures down to a scale of about 5 m. Using the covariance technique, fluxes of sensible (H_s) and latent (H_l) heat and stress (τ) were calculated along each leg. Only the first two quantities will be discussed here. Measurements should be made along 60 km legs in homogeneous conditions to ensure adequate statistical sampling. However, because of the presence of the two frontal features, this was impossible and the warm sector legs were only about half the desired length.

The results of the P-3 flux stack in the offshore warm sector are summarized in Table 1. The boundary layer depth is approximately 600 m, as seen by the profile of virtual potential temperature (θ_v) and the specific humidity (q). The wind speed also shows a maximum near this height. Hence, the surface layer, where the fluxes should be approximately constant with height, is only about 60 m deep, so the lowest flux leg is near the top of this constant flux layer. The fluxes are not constant with height within the rest of the boundary layer, as can be seen.

The effect of the surface fluxes on the boundary layer as it moves towards the coast was estimate by two methods. In the first method, we assume that the fluxes below 66 m are the same

Table 1: *Flux measurements in the offshore warm sector. The values are means for the 26-34 km long legs, where the length is given by "xs-xe". The surface temperature is given by an airborne expendable bathythermograph(AXBT) and the downward-looking radiometer, while the surface mixing ratio is computed assuming saturated conditions.*

Time	Height	xs-xe	<p>	<T>	<q>	$<\theta_v>$	$<\theta_e>$	<ws>	<wd>	H_l	H_s	τ
UTC	m	km	mb	C	g/kg	K	K	m/s	deg	W/m^2	W/m^2	N/m^2
152016 AXBT	0	96		15.73				0	-	-	-	-
155250-155700	0	69-98	993.6	15.8	11.44	291.5	321.7	0	-	-	-	-
155250-155700	66	69-98	985.7	14.9	9.47	290.9	316	13.4	198	32.1	12.1	0.09
153100-153518	285	75-102	960.5	13.15	9.09	291.2	315.4	14.8	197	42	-6	0.05
151900-152400	427	70-104	944.3	12.29	8.89	291.7	315.4	15.6	195	113.6	-47	0.19
145300-145700	590	76-102	926.5	11.22	8.38	292.1	314.6	16.6	198	2.5	-12.1	0.06
144600-145000	1154	73-102	866.6	8.1	6.95	294.2	313.2	13.9	194	32	6	-0.03

Table 2: *Warm sector changes in specific humidity (q) and temperature (T) based on observed fluxes for each layer and for the entire 600 m deep boundary layer. For the entire boundary layer, results from the weighted-mean (WM) and the first layer (L1) methods are shown.*

Height layer (m)	Mean height (m)	Δq (g/kg/2.5 hr)	ΔT (K/2.5 hr)
0-66	33	0.00	0.00
66-285	175.5	-0.14	0.62
285-427	356	-1.51	2.15
427-590	508.5	2.04	-1.60
590-1154	872	-0.16	-0.24
0-600 (WM)	300	0.15	0.31
0-600(L1)	300	0.16	0.06

as at 66 m, and that the fluxes at the different heights remain constant in time as the air parcel translates towards the coast. The flux divergence for each layer then gives the change for that layer, and the average change of a parameter for the entire boundary layer is the layer-weighted mean of the changes over the depth of the boundary layer. The changes for each layer and for the entire boundary layer using this method are seen in Table 2.

The second method assumes that the surface fluxes are given by those measured at 66 m, and that the fluxes are approximately zero at the top of the boundary layer. Hence, the flux divergence and the mean change in the boundary layer can be calculated. These results are given as (L1) in Table 2. Both methods give nearly identical results for the specific humidity; that is, that the boundary-layer specific humidity increases by only about 0.15-0.2 g kg^{-1}. The temperature is expected to increase by either 0.06°C or 0.31°C. The larger discrepancy between the methods for temperature is likely due to the significant role of downward sensible heat flux near the top of the boundary layer. Though the WM method is probably the more accurate, the L1 method is the one that most represents the effects from surface fluxes and will therefore be the one used in the subsequent discussions.

These increases are small values, and would only produce a 0.1-0.3 K and 0.5-0.8 K increase in θ and θ_e, respectively. A shallower boundary layer would produce proportionally greater increases, but the data does not argue for this. However, the fluxes could increase somewhat as the air approaches the shore, since the SST increases slightly shoreward. Therefore, we estimate that an increase of 1 K in θ_e occurs along the trajectory to the coast. The cross-section in the Santa Barbara Channel shows that the maximum warm sector θ_e just ahead of the secondary cold front is 317 K (Fig. 2b), a one degree increase from that measured with the same airborne instruments 2-2.5 hours earlier and shown in Fig. 2a. In addition, the peak θ_e value of 318 K just to the west of the blocking front in Fig. 2b is 1 K greater than that in the corresponding location in Fig. 2a. This remarkable agreement may be fortuitous, although the fact that the airborne verification data was obtained at the right time at the right location for the estimated landfall of the sampled upwind air parcel lends strong credence to this result. Another perspective shows that the additional moisture added during this final 140-km transit to the coast over the warmer coastal water is only 1-2% of the total water content of the air arriving at the coast. Hence, the direct contribution to the coastal precipitation appears to be small.

However, the warming and moistening of the lowest few hundred meters may make a larger impact on destabilizing the air being forced to ascend the steep coastal mountains. We compute the convective available potential energy (CAPE) from the offshore dropsondes and low-level aircraft measurements, and the nearshore CAPE

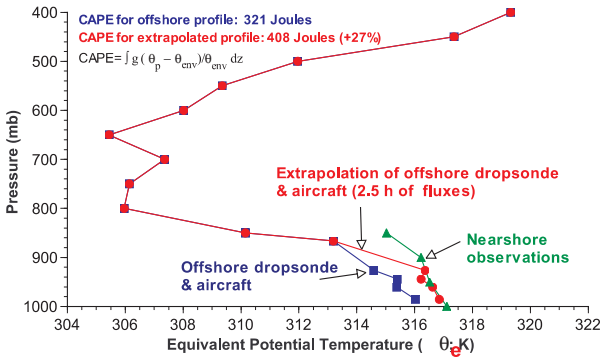

Fig. 4: Profiles of equivalent potential temperature (θ_e) for the offshore location (blue squares), extrapolation to the nearshore location using boundary layer changes due only to surface fluxes (red squares), and nearshore observations (green triangles). The equation for CAPE and the CAPE calculation results for the offshore and extrapolated nearshore profiles are shown at upper left. θ_p and θ_{env} are the parcel and environmental potential temperatures, respectively.

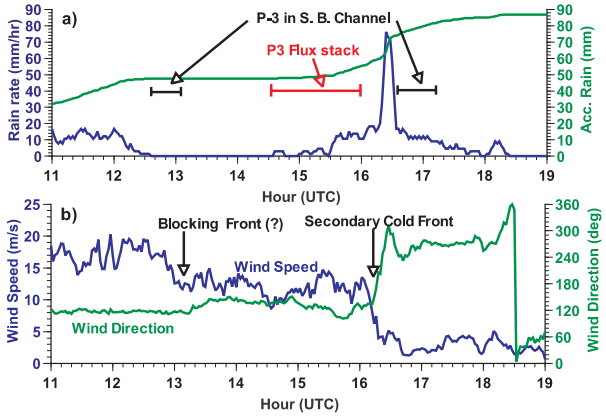

Fig. 5: Surface observations at Goleta. Shown are a) rain rate and accumulated rainfall, and b) wind speed and direction.

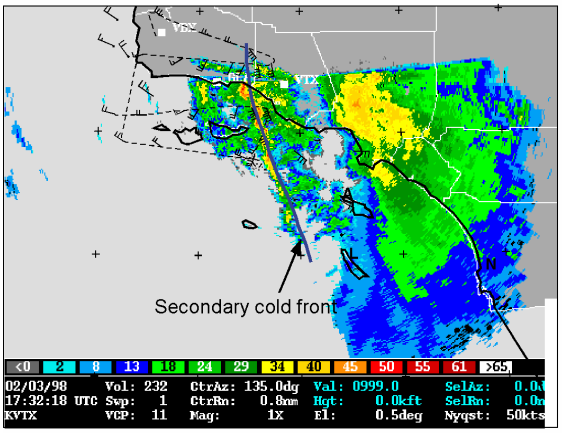

Fig. 6: NEXRAD image from Ventura (VTX) at 1732 UTC Feb. 3. showing the intense convection where the secondary cold front intersects the northern coastline of the California Bight. The front-relative P-3 track is dashed.

Fig. 7: Flooded streets near Goleta airport at about 1800 UTC Feb. 3, 2002. Photo by P. Neiman.

by assuming that the only changes in the sounding occur in the boundary layer and are due to the surface fluxes (Fig. 4). The results show that the 1 K increase of boundary-layer θ_e increases the CAPE by 27% from 321 Joules to 408 Joules. Hence, the coastal surface fluxes substantially decrease the stability and thereby contribute significantly to the very heavy, but brief, precipitation observed at Goleta (Fig. 5) and elsewhere along this part of the California coast (Fig. 6). This period of heavy precipitation resulted in flooding (Fig. 7).

4. EXTENSION TO NON-EL NIÑO YEARS

The above results suggest that coastal surface fluxes did contribute to the heavy coastal precipitation for this event occurring during an El Niño winter. However, what do these results suggest for the influence of coastal fluxes during non-El Niño years?

To examine this question, we utilized the surface flux parameterizations of Fairall *et al.* (1996) to compute the surface H_s and H_l for a range of sea-surface temperatures which included

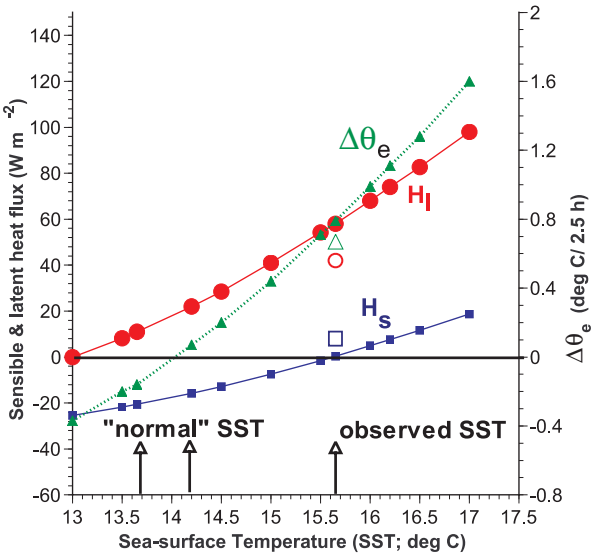

Fig. 8: Sensible heat flux (blue line), latent heat flux (red line), and associated change in the boundary layer θ_e (green line) as a function of sea-surface temperature (SST). The computations of H_s, H_l and $\Delta\theta_e$ were done using the bulk algorithm of Fairall et al *(1996) and assuming conditions as observed in the offshore warm sector on Feb. 3 (z=66 m, ws=13.4 m/s, T=14.9°C, RH=87%, p=985.7 mb, zi=600 m). Also shown are the observed covariance H_s (open blue box), H_l (open red circle) and $\Delta\theta_e$ (open green triangle). The observed SST and those from more normal years are marked by arrows along the bottom.*

both the observed El Niño values and the values typical for non-El Niño years (Fig. 8). In these computations, we assume that the boundary-layer conditions were the same as that observed for the Feb. 3 case. The expected 2.5-hour change in θ_e is then computed.

The results for the observed El Niño conditions show that the parameterization does a good job at predicting the observed surface fluxes and the change in boundary-layer θ_e (Fig. 8). Hence, the model appears reliable. For SSTs representative of non El Niño years, the H_s was substantially negative and the H_l was positive but smaller. Hence, the change in θ_e is predicted to be near zero or slightly negative. That is, the coastal surface fluxes are not expected to contribute to the destabilization of the boundary layer during landfalling storms in a non El Niño year, even though they do contribute during El Niño years. They might even lead to slight stabilization.

5. CONCLUSIONS

This paper uses the case of February 3, 1998, to show that the observed surface sensible and latent heat fluxes within 150 km of the shore within a moderate low-level jet can significantly contribute to the destabilization of the air just before it is forced to ascend at the cold front and the steep coastal terrain. As the air ascends, deep convection occurs with significant coastal flooding as result. A bulk surface flux parameterization is shown to match direct surface flux measurements reasonably well in this case, and is used to extend the results to suggest that the coastal fluxes only enhance the coastal precipitation during years with anomalously warm coastal sea-surface temperatures (ENSO years) and may even help suppress coastal convection during years of more normal colder SSTs.

Though this is only one case and the effect of surface fluxes vary from storm to storm, these results serve to illustrate a point. During El Niño years when coastal waters are anomalously warm by 1.5-2°C, surface heat fluxes near the California coast can contribute to the coastal precipitation. During non-El Niño years, they are much less likely to do so unless the air temperatures in the storms are significantly colder.

6. REFERENCES

Fairall, C. W., E. F. Bradley, D. P. Rogers, J. B. Edson, and G. S. Young, 1996: Bulk parameterization of air-sea fluxes for Tropical Ocean-Global Atmosphere Coupled-Ocean Atmosphere Response Experiment, *J. Geophys. Res.*, **101**, 3747-3764.

Kuo, Y.-H., and R. J. Reed, 1988: Numerical simulation of an explosively deepening cyclone in the eastern Pacific. *Mon. Wea. Rev*., **116**, 2081-2105.

Kuo, Y.-H., R. J. Reed, and S. Low-Nam, 1991: Effects of surface energy fluxes during the early development and rapid intensification stages of seven explosive cyclones in the western Atlantic. *Mon. Wea. Rev.*, **119**, 457-476.

Langland, R. H., R. L. Elsberry, and R. M. Errico, 1995: Evaluation of physical processes in an idealized extratropical cyclone using adjoint techniques. *Quart. J. Roy. Meteor. Soc.*, **121**, 1349-1386.

Neiman, Paul J., F. M. Ralph, P. O. G. Persson, A. B. White, D. P. Jorgensen, and D. E. Kingsmill, 2002: The influence of coastal orography on a high-impact land-falling winter storm in Southern California: Observations during CALJET. To be submitted to *Mon. Wea. Rev*.

Persson, P. O. G, P. Neiman, F. M. Ralph, B. Walter, J.-W. Bao, S. Michelson, D. Jorgensen, and J. Schmidt, 1999: Measurements and modeling of air-sea interaction processes prior to heavy coastal precipitation: The case of Feb. 3, 1998. *Proceedings, Third Conf. On Coastal Atmospheric and Oceanic Prediction and Processes*, New Orleans, LA, Nov. 1999b.

Persson, P. O. G., F. M. Ralph, B. Walter, P. Neiman, C. King, A. White, and J. Wilczak, 1999: Observations of the structure of the low-level jet in landfalling winter storms using the CALJET observational network. *Preprints, 3rd Symp. on Integrated Observing Systems*., Jan. 10-15, 1999a, Dallas, TX, 82-85.

Ralph, F. M., P. O.G. Persson, D. Reynolds, W. Nuss, D. Miller, J. Schmidt, D. Jorgensen, J. Wilczak, P. Neiman, J.-W. Bao, D. Kingsmill, Z. Toth, C. Veldon, A. White, C. King,, and J. Wurman, 1999a: The California Land-falling Jets Experiment (CALJET): Objectives and design of a coastal atmosphere-ocean observing system deployed during a strong El Niño. *Preprints, 3rd Symp. on Integrated Observing Systems*., Jan. 10-15, 1999, Dallas, TX, 78-81.

Reed, R. J., and M. D. Albright, 1986: A case study of explosive cyclogenesis in the eastern Pacific. *Mon. Wea. Rev.,* **114**, 2297-2319.